Effects of pressure and magnetic field on superconductivity in $ZrTe_3$: local pair-induced superconductivity

2017 New J. Phys. 19 063004

(http://iopscience.iop.org/1367-2630/19/6/063004)

New Journal of Physics
The open access journal at the forefront of physics

Deutsche Physikalische Gesellschaft DPG
IOP Institute of Physics

Published in partnership with: Deutsche Physikalische Gesellschaft and the Institute of Physics

OPEN ACCESS

RECEIVED
23 January 2017

REVISED
3 April 2017

ACCEPTED FOR PUBLICATION
13 April 2017

PUBLISHED
2 June 2017

PAPER

Effects of pressure and magnetic field on superconductivity in $ZrTe_3$: local pair-induced superconductivity

S Tsuchiya[1,2], **K Matsubayashi**[2,3], **K Yamaya**[1], **S Takayanagi**[1], **S Tanda**[1,4] **and Y Uwatoko**[2]

[1] Department of Applied Physics, Hokkaido University, Sapporo, Hokkaido 060-8628, Japan
[2] Institute for Solid State Physics, The University of Tokyo, Kashiwa, Chiba 277-8581, Japan
[3] Department of Engineering Science, The University of Electro-Communications, Chofu, Tokyo 182-8585, Japan
[4] Center of Education and Research for Topological Science and Technology, Hokkaido University, Sapporo, Hokkaido 060-8628, Japan

E-mail: satoshi.tsuchiya@eng.hokudai.ac.jp

Keywords: superconductivity, magnetic field, pressure

Abstract

In this work, the origin of the highly anisotropic superconducting transition in $ZrTe_3$, where the resistance along the a axis, R_a, is reduced at 4 K but those along the b axis, R_b, and c' axis, $R_{c'}$, are reduced at 2 K, was explored with the application of a magnetic field and pressure by the electrical resistance measurements. We found that the behavior of the upper critical field and its anisotropy as well as the pressure dependence determined by the R_a measurements are quite similar to those of R_b. Moreover, the excess conductivity for R_b indicates anomalous behavior. These results support an unconventional origin for the anisotropic transition rather than conventional superconducting fluctuation. The reduction in R_a is due to filamentary superconductivity (SC) induced by locally bound electron pairs (local pairs), which correspond to bi-polarons, and the transition of R_b corresponds to the emergence of bulk SC originating from the Cooper pairs triggered by the transfer of the local pairs.

1. Introduction

Up to now, the coexistence and competition between charge density waves (CDWs) and superconductivity (SC) have been a major research topic in the field of condensed matter physics. Indeed, CDW transitions have been observed in low-dimensional materials such as transition-metal di- and trichalcogenides [1–4], which have chain and layered crystal structures, as well as cuprates [5–8]. Many compounds exhibit SC behavior at low temperatures in the CDW ordering state [9, 10]. In some cases, the CDW and SC states are suppressed or enhanced by pressure, indicating that their peculiar electronic structures due to low dimensionality can play a crucial role with regard to CDW and SC coexistence and competition. It is of interest and value to reveal the mechanism of such CDWs and SC.

Among these compounds, $ZrTe_3$ has attracted considerable attention owing to its unique electronic structures, which originate from the low dimensionality of the crystal structure [11, 12]. Strikingly, when the temperature is reduced below the CDW transition temperature T_{CDW} (=63 K), a highly anisotropic resistive transition in the SC has been observed. The resistance R_a along the a axis starts to decrease at 4 K, whereas the resistances R_b and $R_{c'}$ along the b and c' axis, respectively exhibit relatively rapid reductions at 2 K [13, 14]. Since magnetic measurements have shown that a diamagnetic signal is not observed down to 2 K [14], the reduction of R_a can arise from filamentary SC rather than bulk SC. This unusual behavior can be explained by two scenarios, conventional superconducting fluctuation and SC induced by locally bound electron pairs (local pairs). In the former, the reduction in R_a is attributed to a fluctuation in the bulk SC enhanced by the low dimensionality. In the latter, the transitions of R_a and $R_{b,c'}$ correspond to filamentary and bulk SC, which originate from the formation of local pairs, namely bi-polarons, and Cooper pairs induced by the transfer of the local pairs, respectively, owing to a peculiar electronic structure after the CDW transition [15]. At this moment, it remains unclear which interpretation is acceptable. Moreover, although formation of the local pairs has been discussed as

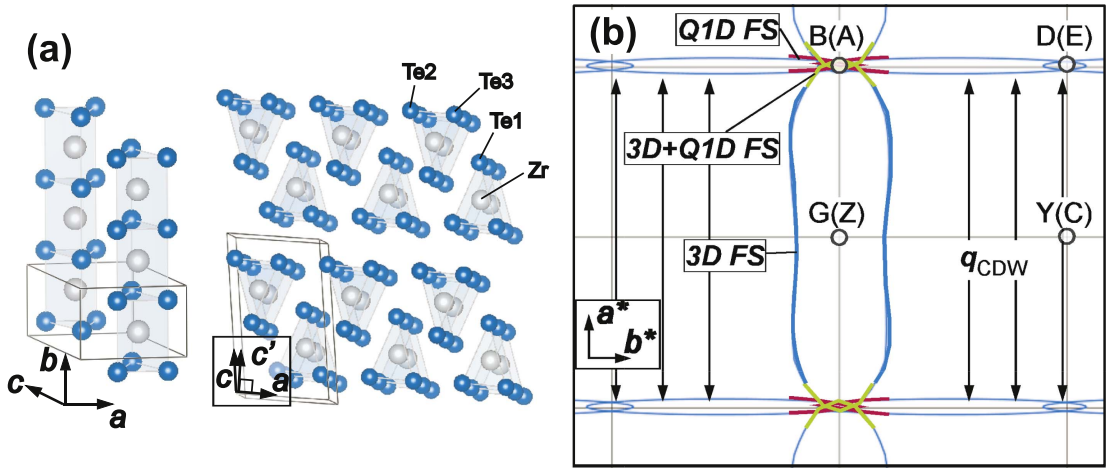

Figure 1. (a) Schematic of $ZrTe_3$ crystal structure. The unit cell parameters are $a = 5.8948$ Å, $b = 3.9264$ Å and $c = 10.109$ Å and $\beta = 97.32°$ [11]. (b) Schematic of $ZrTe_3$ Fermi surface [12].

a possible mechanism of high-temperature SC for a long time [16–18], experimental indications are still limited. In this sense, investigations on SC in $ZrTe_3$ can provide important insights regarding the presence of local-pair induced SC.

To understand SC in more detail, we discuss the influence of pressure and the magnetic field on the SC in $ZrTe_3$, as determined via R_a and R_b measurements. The experimental results are shown in section 3. In section 3.1, the pressure–temperature (P–T) phase diagram is constructed. The behaviors of the upper critical fields H_{c2} are discussed using the Ginzburg–Landau (GL) theory in sections 3.2 and 3.3. We found that the temperature and pressure dependences of H_{c2} obtained by R_a measurement is similar to those obtained by R_b measurement. Moreover, to explore the peculiar properties of the filamentary SC, the H_{c2} curves and H_{c2} anisotropy are assessed with several models based on the GL theory. Additionally, in the analysis of the superconducting fluctuation with the Aslamazov and Larkin (AL) theory (section 3.4), the excess conductivity of R_b seems to have a one-dimensional (1D) character, although the bulk SC is observed in this current configuration. As discussed in section 4, by taking into consideration previous studies, we conclude that our results indicate unconventional origins for the anisotropic superconducting transition, which is attributed to local-pair-induced SC rather than conventional superconducting fluctuation.

2. Experimental

Single crystals of $ZrTe_3$ were prepared using the iodine (I_2) vapor transport method [15]. The crystal structure is shown in figure 1(a). Chains consisting of $ZrTe_3$ prisms formed along the b axis. In the figure, upright and inverted chains are alternately arranged along the a axis, forming layers. The layers are stacked perpendicularly to the ab plane (along the c' axis), where the c' axis is tilted slightly from the c axis because of the monoclinic crystal structure. Band structure calculations predicted quasi-one-dimensional (Q1D) Fermi surface (FS) sheets, a three-dimensional (3D) sheet, and a van Hove singularity (vHS), which consists of the intersection of Q1D and 3D (Q1D+3D) FSs, [12] as shown in figure 1(b).

The electrical resistivity was measured using a standard four-terminal method. The typical crystal sizes used in the experiments conducted in this study were $1 \times 0.5 \times 0.01$ mm^3. Four gold wires 20 μm in diameter were attached to the cleaved surfaces of the samples using carbon paste. To detect the anisotropic SC transition, R_a and R_b were measured with 0.1 mA of AC current directed along the a axis for samples ♯1 and ♯3 and along the b axis for ♯2 and ♯4, respectively. For the measurements conducted under ambient pressure, ♯1 and ♯2 were mounted on the same sample holder and the data were recorded simultaneously. For the pressure measurements, samples ♯3 and ♯4 and lead (Pb), which was used as the manometer [19], were set in a piston-cylinder-type pressure cell with the pressure medium (Daphne 7373). The experiments were carried out using ^{3}He and dilution refrigerators with an SC magnet.

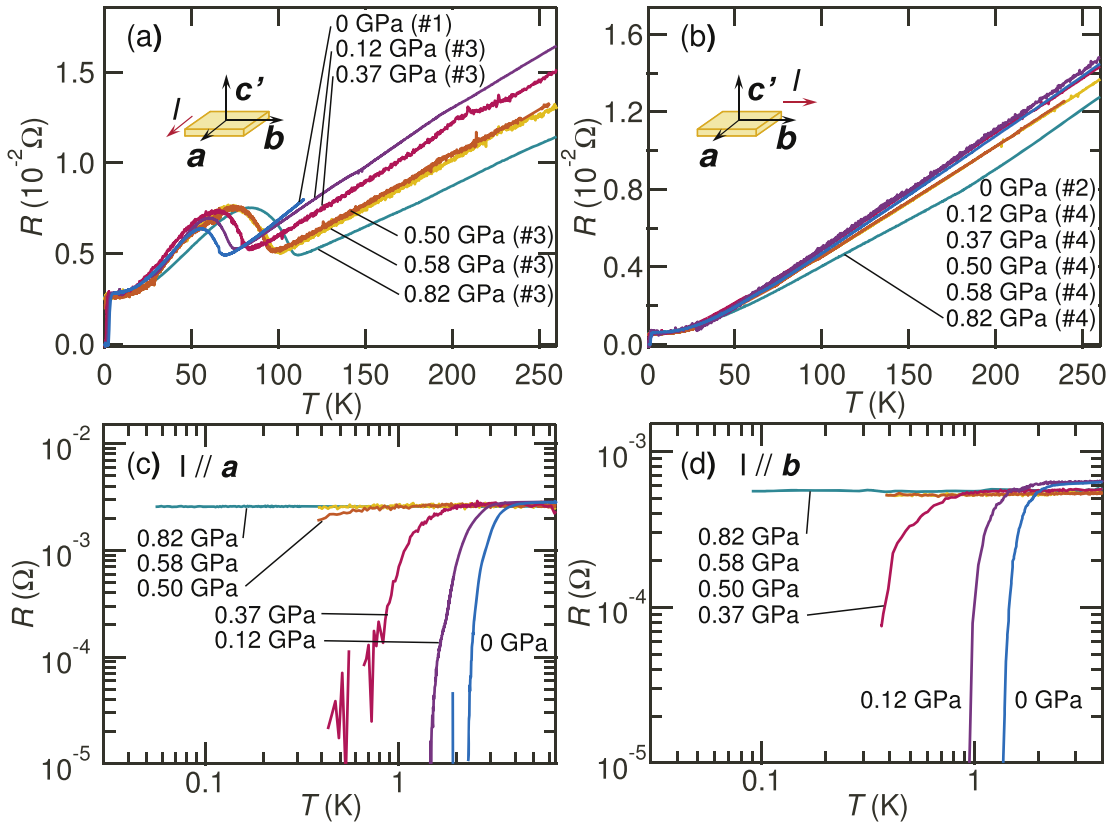

Figure 2. (a), (b) Temperature dependence of resistance for various pressures in $I \parallel a$ (♯1 and 3) and $I \parallel b$ (♯2 and 4), respectively. (c), (d) Temperature dependence of resistance in low temperature region on logarithmic scales.

3. Results

3.1. *P–T* phase diagram

At room temperature, the resistivities of all $ZrTe_3$ samples were roughly estimated under 0 kbar. as 1.5, 1.0, 0.4 and 1.0 $\times$ $10^{-6}\,\Omega\,m^{-1}$ for ♯1–♯4, which are in good agreement with those of the previous report [20]. Figures 2(a) and (b) show the temperature dependence of the R_a and R_b under various pressures, respectively. For $I \parallel a$, the resistance reduced with decreasing temperature and then suddenly increased at approximately 70 K. No visible anomaly was observed for $I \parallel b$. This behavior is attributed to the CDW transition. Further, as the CDW forms along the direction between the *a* and *c* axes [21], the anomaly in the R_b is extremely small [14]. In this study, when pressure was applied, T_{CDW} shifted to the high-temperature side.

Figures 2(c) and (d) show the R_a and R_b at various pressures in the low-temperature region, respectively, which are plotted as a function of temperature on a log scale. For 0 GPa, the R_a drops to zero at 2.2 K, while the R_b decreases to zero at 1.4 K. The highly anisotropic SC transitions are reflected by the filamentary and bulk nature of the SC. Note that the filamentary SC occurs along the *a* axis and no visible anomaly in the specific heat [15]. On the other hand, the zero resistance for $I \parallel b$ at 1.4 K corresponds to the bulk SC transition, where a specific heat anomaly has previously been observed [15]. For $I \parallel a$, the small drops of resistance were observed at 0.50 GPa. At 0.82 GPa, however, no reductions in resistance were observed, even at temperatures lower than 0.1 K. On the other hand, for $I \parallel b$, no resistance drops were observed at pressures higher than 0.50 GPa.

A *P–T* phase diagram can be constructed from the above data, as shown in figure 3. Note that T_{CDW} was defined as the onset temperature of the resistance anomaly. For the SC transition, we defined T_c(onset) and $T_c(R = 0)$ as the intersection between the extrapolation from the high temperatures and the tangent line at half of the normal state resistance, and the extrapolation of the tangent line to zero resistance, respectively, as shown in the inset of figure 4(c). As the pressure was increased, T_{CDW} also increases, while the T_c of the filamentary SC reduced; these results conform to behavior reported in the previous study [22]. This behavior and the resistivity agreement at room temperature ensure measurement reproducibility of the measurements. Strikingly, the T_c of the bulk SC also decreases in the same manner as that of the filamentary SC. This means that the origin of the bulk SC can be related to that of the filamentary SC. Moreover, as T_c seems to be negatively correlated with the T_{CDW}, both the SC phases can compete with the CDW phase.

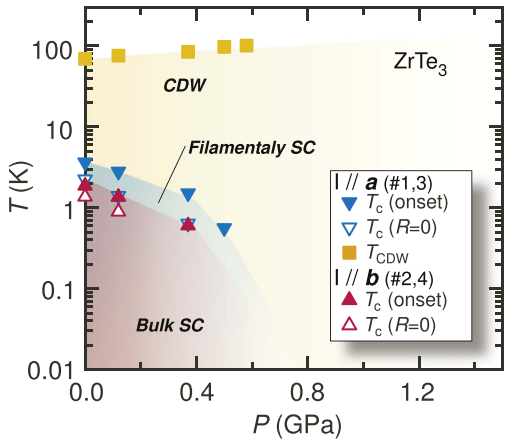

Figure 3. Temperature-pressure phase diagram of $ZrTe_3$. The triangles and squares indicate T_c and T_{CDW}, respectively. The closed and open symbols indicate the T_c determined by the onset and resistance drop temperatures, respectively.

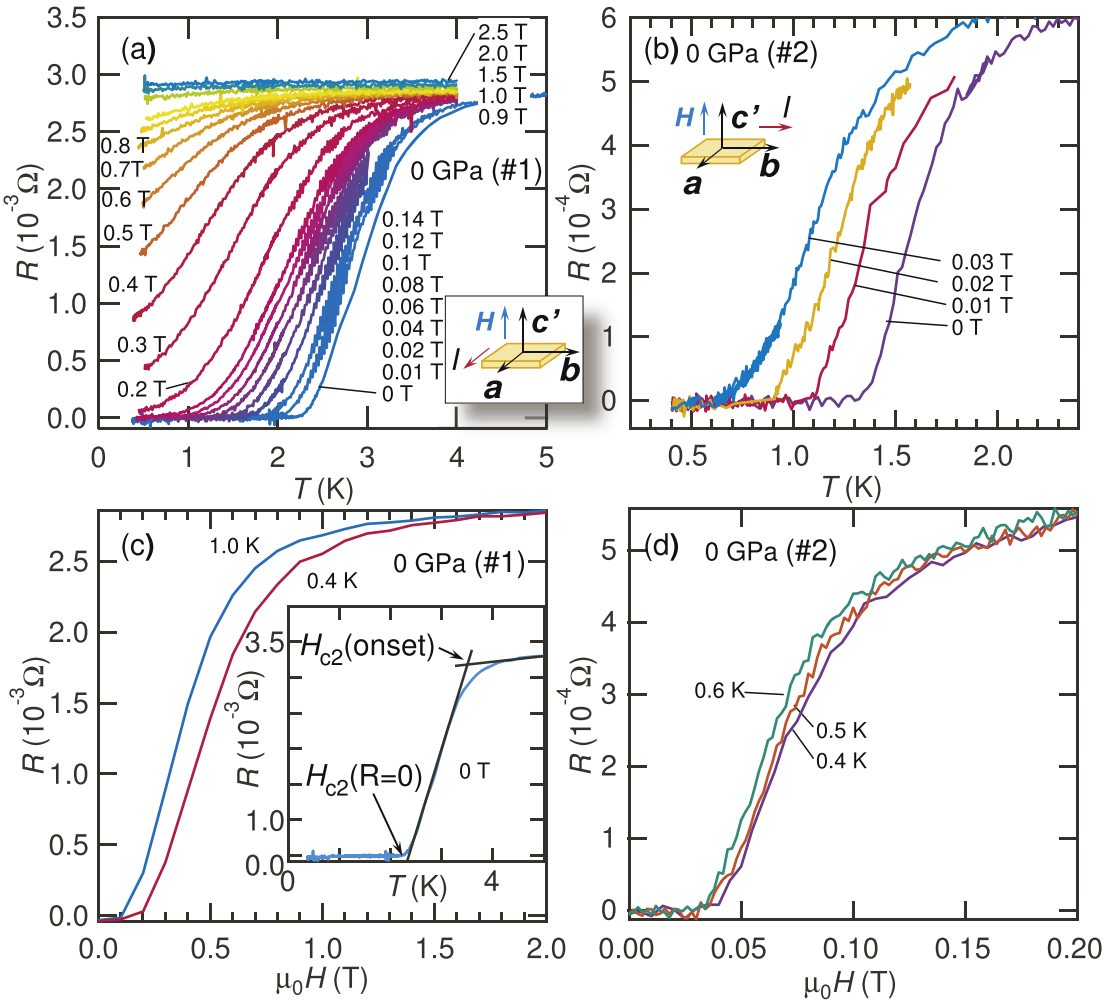

Figure 4. (a), (b) Temperature dependence of resistance under various magnetic fields for $I \parallel a$ (♯1) and $I \parallel b$ (♯2), respectively. (c), (d) Magnetic-field dependence of resistance under various magnetic fields for $I \parallel a$ (♯1) and $I \parallel b$(♯2), respectively. The inset shows the definition of H_{c2}(onset) and $H_{c2}(R = 0)$.

3.2. Upper critical fields

Figures 4 (a) and (b) show the temperature dependence of R_a and R_b, respectively, for various magnetic fields, which were applied with respect to the *ab* plane (along the c' axis) under ambient pressure. When the magnetic field increases above 0.2 T for $I \parallel a$, T_c is shifted to the low temperature side and the transition became broad.

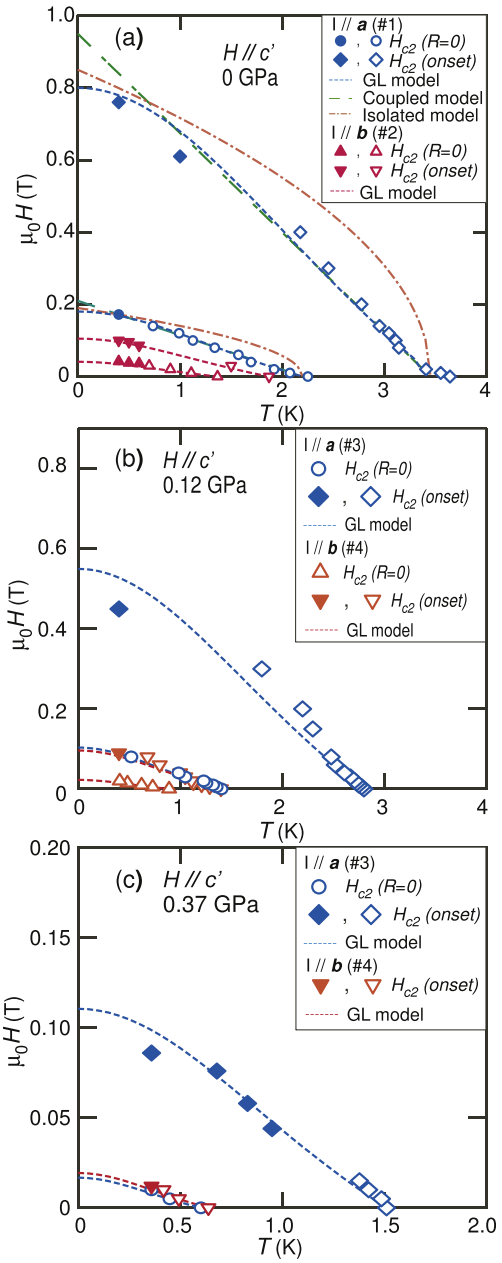

Figure 5. (a), (b), (c) Phase diagram of $ZrTe_3$ for the magnetic field $H // c$ under $P = 0$, 0.12 and 0.37 GPa, respectively. Circles and diamonds indicate $H_{c2}(R = 0)$ and H_{c2}(onset) for $I \parallel a$, respectively. Triangles indicate $H_{c2}(R = 0)$ and H_{c2}(onset) for $I \parallel b$. Closed and open symbols mean that H_{c2} is determined by use of the magnetic field and temperature dependence measurements, respectively. Dashed, dashed-one dotted, and dashed-two dotted lines indicate the results of fitting of the GL, coupled filament SC, and isolated filament SC model, respectively.

Moreover, for $I \parallel b$, T_c decreases with increasing magnetic field. Figures 4 (c) and (d) show the magnetoresistance results for several temperatures for $I \parallel a$ and $I \parallel b$, respectively. For $I \parallel a$, the resistance curve exhibits a steep increase at magnetic fields 0.2 T at 0.4 K, while for $I \parallel b$, this increase occurs for magnetic fields above 0.04 T. Using the criteria shown in the inset of figure 4(c), we defined the upper critical field H_{c2}(onset) and $H_{c2}(R = 0)$. Figure 5(a) shows the phase diagram for $H \parallel c'$. The open and closed symbols represents the H_{c2} derived from the temperature and the magnetic-field dependence measurements, respectively.

The upper critical field can be associated with two different types of suppression mechanism of SC, i.e. the Pauli paramagnetic and orbital effects. In the former mechanism, the SC states are broken by Zeeman splitting for spin singlet pairings [23]. For Bardeen–Cooper–Schrieffer (BCS) superconductors, the Pauli paramagnetic limit can be obtained as $H_P = \Delta/\sqrt{2}\mu_B = 1.84T_c$, where μ_B is the Bohr magneton and $\Delta = 1.76k_B T_c$ is the BCS energy gap in the weak coupling limit. For example, by substituting $T_c = 3.4$ K for H_{c2}(onset) with $I \parallel a$, $\mu_0 H_P$ is estimated as 6.07 T, which is significantly larger than the H_{c2}(onset) value of ~0.9 T obtained from linear extrapolation to $T = 0$ K. On the other hand, in the latter case, the SC is suppressed by increased kinetic energy

Table 1. Slopes of H_{c2} curve near T_c (dH/dT), T_c, and $H_{c2}^{orb}(0)$ for $P = 0$, 0.12, and 0.37 GPa, respectively.

		0 GPa				0.12 GPa			0.37 GPa		
		T_c (K)	$\left(\frac{\mu_0 dH}{dT}\right)_{T=T_c}$ (T K^{-1})	$H_{c2}^{orb}(0)$ (T)	H_P (T)	T_c (K)	$\left(\frac{\mu_0 dH}{dT}\right)_{T=T_c}$ (T K^{-1})	$H_{c2}^{orb}(0)$ (T)	T_c (K)	$\left(\frac{\mu_0 dH}{dT}\right)_{T=T_c}$ (T K^{-1})	$H_{c2}^{orb}(0)$ (T)
$I//b$	$H_{c2}(R=0)$	1.37	−0.043	0.04	2.52	0.9	−0.021	0.02	—	—	—
	H_{c2}(onset)	1.87	−0.081	0.11	3.44	1.4	−0.074	0.096	0.63	−0.043	0.019
$I//a$	$H_{c2}(R=0)$	2.2	−0.11	0.18	4.14	1.4	−0.064	0.10	0.6	−0.041	0.017
	H_{c2}(onset)	3.4	−0.341	0.80	6.07	2.8	−0.241	0.55	1.5	−0.106	0.11

due to the orbital current to exclude the magnetic field. The upper critical field determined by the orbital effect at $T = 0$ K is given by [24]

$$\mu_0 H_{c2}^{orb}(0) = -0.69 T_c \left(\frac{\mu_0 dH_{c2}}{dT}\right)_{T=T_c}, \quad (1)$$

where $\frac{\mu_0 dH_{c2}}{dT}$ is the initial slope at T_c. For H_{c2}(onset) with $I \parallel a$, $\frac{\mu_0 dH_{c2}}{dT} \sim -0.341$, which provides $H_{c2}^{orb}(T=0) \sim 0.8$ T. The H_{c2} curve was fitted using this value and the empirical expression based on the GL theory [25], which provides the phase boundary determined by the orbital effect. The GL expression is expressed as

$$H_{c2}(T) = H_{c2}^{orb}(0)\frac{1-t^2}{1+t^2}, \quad (2)$$

where t is the reduced temperature T/T_c. The results of the calculations are in good agreement with the H_{c2}(onset) and $H_{c2}(R=0)$ curves for $I \parallel a$ and $I \parallel b$ over the entire temperature range, as shown in figure 5(a). The $\mu_0 H_P$ and $\mu_0 H_{c2}^{orb}(T=0)$ results for all the H_{c2}(onset) and $H_{c2}(R=0)$ values are summarized in table 1. These results indicate that the orbital effect is dominant for suppression of both the bulk and filamentary SC, when a magnetic field is applied.

To investigate the filamentary SC further, the H_{c2} curves were compared with those predicted by a model based on GL theory [26]. This theory proposes two types of filamentary SC, where the SC filaments are either coupled or isolated. In the former case, the SC filaments interact via the Josephson coupling and the I paths can be enclosed. As a result, H_{c2} is expected to be proportional to $|(T - T_c)/T_c|$ near T_c. On the other hand, SC filaments are decoupled in the latter case. Thus, the screening I path is not enclosed, leading to suppression of the orbital effect. In that case, H_{c2} is proportional to $|(T - T_c)/T_c|^{1/2}$. Therefore, the difference between these two types of filamentary SC is most significantly pronounced near T_c. As shown by the plot in figure 5(a), the coupled model fits the obtained data more closely than the isolated model. Further, the deviation between the coupled model and our data at low temperatures is irrelevant because the models are valid near T_c only.

The H–T phase diagrams obtained under 0.12 and 0.37 GPa are shown in figures 5(b) and (c), respectively. The H_{c2} curves are quite similar to that for 0 GPa and fit the GL expression (equation (2)) well. Therefore, the suppression mechanism of SC for application of the magnetic field is unchanged by pressure. All the $\frac{\mu_0 dH_{c2}}{dT}$ and $H_{c2}^{orb}(0)$ values are also summarized in table 1.

3.3. Angular dependence of H_{c2}

For the filamentary SC, the angular dependence of H_{c2} was measured. Figure 6(a) shows the magnetic-field dependence of the resistance for various angles at 0.4 K under 0 GPa. The field angle ϕ was defined as the angle between the b axis and magnetic field, as shown in the inset of figure 6(b). When the magnetic field was tilted from the 90° direction ($H \parallel c'$), the resistive transition was shifted to the high-field side. Figure 6(b) shows the ϕ dependence of $H_{c2}(R=0)$ for $I \parallel a$. The $H_{c2}(R=0)$ values in the vicinity of 0° are approximately two times greater than those at high ϕ, indicating anisotropic SC. We tentatively compared the data with two different theoretical models, the anisotropic GL (AGL) model [27] and the two-dimensional (2D) model. For the AGL model, the anisotropy of SC is included as that of H_{c2} or the effective mass. The ϕ dependence of H_{c2} is described as

$$\left(\frac{H_{c2}(\phi)\cos(\phi)}{H_{c2}^{\perp}}\right)^2 + \left(\frac{H_{c2}(\phi)\sin(\phi)}{H_{c2}^{\parallel}}\right)^2 = 1, \quad (3)$$

where $H_{c2}^{\perp}$ and $H_{c2}^{\parallel}$ are the upper critical fields for the perpendicular and parallel field directions relative to SC layers, respectively. On the other hand, in the case of 2D superconductors, the layers of which are connected via Josephson coupling, the ϕ dependence of the critical field is given by [28]

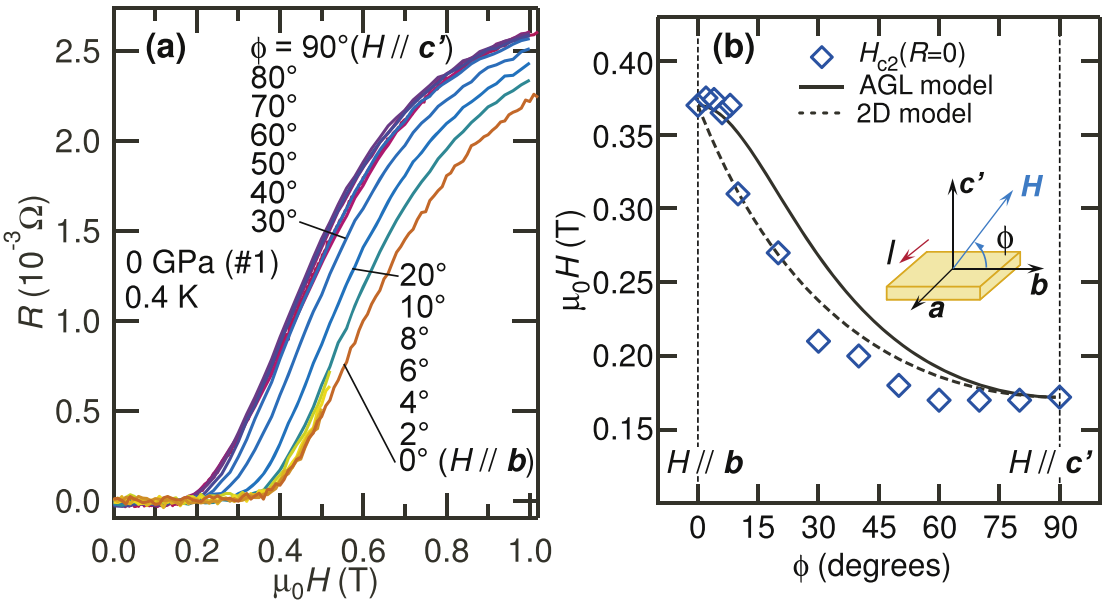

Figure 6. (a) Magnetic-field dependence of resistance for various ϕ at 0.4 K under 0 GPa. (b) Angular dependence of $H_{c2}(R = 0)$ for $I \parallel a$. The inset shows the definition of ϕ.

$$\left| \frac{H_{c2}(\phi)\cos(\phi)}{H_{c2}^{\perp}} \right| + \left(\frac{H_{c2}(\phi)\sin(\phi)}{H_{c2}^{\parallel}} \right)^2 = 1. \tag{4}$$

The solid and dotted curves in figure 6(b) correspond to the calculated results of the AGL and 2D models, respectively. At low ϕ, the $H_{c2}(R = 0)$ values are close to those of the AGL model (equation (3)), but tend to agree with the 2D model (equation (4)) at high ϕ. Remarkably, the anisotropy direction, as well as the $\gamma = H_{c2}^{\parallel}/H_{c2}^{\perp} \sim 2.2$ in the filamentary SC, agree reasonably well with the result of $\gamma \sim 3$ obtained for the bulk SC [14], indicating similarity between the filamentary and bulk SCs.

To explore the peculiar properties of the filamentary SC, we compared the azimuthal ϕ dependence data with the theoretical model [26]. As the filamentary SC model is very simple [26], it can provide useful clues concerning the behavior of the filamentary SC. In the case that SC filaments are arranged in a rectangular lattice, H_{c2} is expected to exhibit a unique ϕ dependence of H_{c2}, with a minimum value for the azimuthal angle $\phi = 45°$ well below T_c. This behavior corresponds to variation of H_{c2} with a 90° period. On the other hand, near T_c, the ϕ dependence is identical to that of the AGL model (equation (3)). In our results for $T/T_c \sim 0.4$ (figure 6), H_{c2} varied with a 180° period which is consistent with the AGL model. This can indicate that the SC filaments cannot be arranged regularly.

3.4. Excess conductivity

To investigate the SC fluctuation, we extracted the excess conductivity from the resistance data. Figures 7 (a) and (b) show the temperature dependence of the normalized excess conductivity $\Delta\sigma/\sigma_0 = (\sigma - \sigma_0)/\sigma_0$, where σ_0 is the conductivity under various pressures, for $I \parallel a$ (at 5 K) and $I \parallel b$ (3 K), respectively. $T_c(R = 0)$ values were used. The $\Delta\sigma/\sigma_0$ curves were found to be qualitatively similar for pressure variations in both current configurations. According to the AL theory [29], the excess conductivity due to SC fluctuation is given by

$$\Delta\sigma_{3D} \propto \left(\frac{T - T_c}{T_c} \right)^{-\frac{1}{2}}, \tag{5}$$

$$\Delta\sigma_{1D} \propto \left(\frac{T - T_c}{T_c} \right)^{-\frac{3}{2}}, \tag{6}$$

for 3D and 1D superconductors, respectively. The dashed lines in figure 7 are calculations for the 3D and 1D cases, which have been included to facilitate a qualitative comparison in the temperature dependence. For $I \parallel a$, the experimental results agree with the 1D AL model, which is consistent with a previous report [30]. For $I \parallel b$, the temperature dependence corresponds to the 1D rather than the 3D model, although the bulk SC is observed in this I configuration.

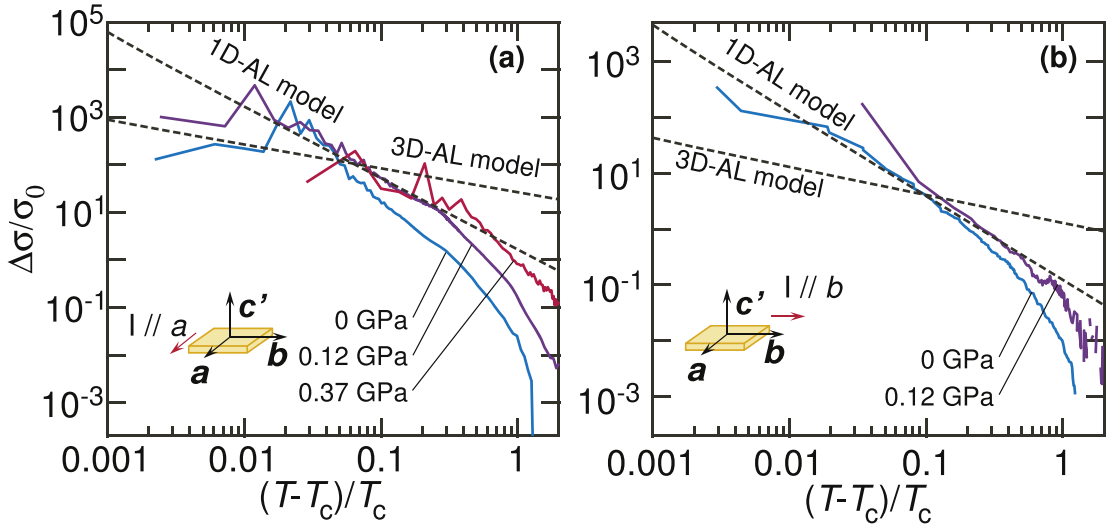

Figure 7. (a), (b) Temperature dependence of normalized excess conductivity for $I \parallel a$ and $I \parallel b$, respectively. The dashed lines indicate the results calculated for 1D and 3D cases using the AL theory.

4. Discussion

We now discuss the origins of the bulk and filamentary SCs from the perspective of the electronic structure. Recent ARPES measurements have shown that the Q1D FSs vanish as a results of the CDW formation (see figure 1(b)) and, simultaneously, a large enhancement in the electronic density of states near the vHS can be observed at the Fermi energy (E_F) below T_{CDW} [31]. As has been shown in figure 3, T_{CDW} increases when the T_c values of both SCs decrease with increasing pressure. This indicates that the remaining Q1D+3D FSs are related to the emergence of the SC, rather than the 3D FSs.

In the band calculations [12], the energy dispersions of the Q1D+3D FSs in the vicinity of the vHS are almost flat, corresponding to $v_F \sim 0$, where v_F is the Fermi velocity. It is known that a vHS at E_F can have FS instabilities that introduce a SC state [32, 33]. If electron pairs of Q1D parts of the FSs are formed, the spatial size of the corresponding wave packet can be estimated based on the Pippard coherence length $\xi_0 \sim \frac{\hbar v_F}{k_B T_c}$, where $\hbar$ and k_B denote the Planck and Boltzmann constants, respectively [25]. As $v_F \sim 0$, ξ_0 is expected to be very small, yielding electron pairs with very short coherence length that tend to be localized. Such local pairs correspond to bi-polarons consisting of electrons bound by strong electron–phonon interaction [16–18]. As they have Bose characters, the local pairs can condense into a SC state analogous to the superfluid state of ^{4}He II [34].

In $ZrTe_3$, the local pairs form along the a axis; this is because Q1D FS consists of electrons in the narrow band originating from the p_x orbitals of the Te(2)–Te(3) chain parallel to the a axis, as has been shown in figure 1(a). With decreasing temperature, local pairs are induced and phase coherence develops gradually, causing broad resistive transition along the a axis. In this manner, the unique electronic structure of $ZrTe_3$ favors SC as a results of the local pair formation.

Furthermore, several theories have predicted that, in the case of narrow-and wide-band hybridization, the local pairs in the narrow band can induce Cooper pairs spontaneously among the electrons of the wide band [16, 17]. In $ZrTe_3$, as the 3D FS is derived from wide-band electrons, such hybridization is realized in the vicinity of vHS [12]. If a large number of local pairs are induced as the temperature decreases, the local pairs of the narrow band are transfered to the wide-band states of the Q1D+3D FSs, inducing Cooper pairs. This behavior yields the bulk SC. In fact, this picture corresponds to a crossover between the filamentary and bulk SC with varying temperature, which explains the anomalous behavior of the specific heat well, as was discussed in a previous report [15].

The inseparable relationship between the two types of SC induced by the local and Cooper pairs is consistent with the implications of our results. As shown in figure 5, the H_{c2} curves of the filamentary SC were quite similar to those of the bulk SC. Moreover, the filamentary SC phase was decreased in the same manner as the bulk phase, when the pressure was increased. As regards the anisotropy of H_{c2}, the direction and γ value of the filamentary SC are in agreement with those of the bulk SC.

In $ZrTe_3$, the onset temperature of R_a is much higher than that of R_b by ~3 K. This behavior indicate that bulk SC coherence is not easy to establish because coupling between the SC filaments is very weak because of a

very short coherence length. This is consistent with their extremely short coherence length of less than 10 Å for the filamentary SC, which suggested by the specific heat measurements [15].

On the other hand, a similar two-stage resistive transition of SC has been reported in the Q1D materials family such as $Tl_2Mo_6Se_6$ and $Na_2Mo_6Se_6$ [35, 36]. As temperature decreases, the resistivity reduces but does not become zero in $Tl_2Mo_6Se_6$. This behavior can be explained by appearance of SC fluctuation owing to a highly 1D crystal structure. When the temperature is lowered further, such 1D SC bundles become coupled with each other and establish 3D phase coherence, showing the zero-resistive transition due to the bulk SC. However, the onset temperature of the SC fluctuation is higher than that of the bulk SC by only ~1 K, indicating that 3D SC correlation develops more easily than it does in $ZrTe_3$. Therefore, the coherence length of the SC fluctuation is expected to be longer than that in $ZrTe_3$. This finding suggests that the filamentary SC in $ZrTe_3$ can arise from the local pairs as a limit for a very short coherence length rather than the ordinary Cooper pairs.

Our results regarding the excess conductivity are in agreement with the 1D AL model rather than the 3D model, for both the *I* configurations. This agreement is reasonable for $I \parallel a$, because the SC channel develops along the *a* axis, indicating that the fluctuation is derived from the highly 1D SC. On the other hand, for $I \parallel b$, the disagreement with the 3D model is unexpected, as the bulk SC can originate from the 3D FS. Similar behaviors have been observed in the cuprates and suggest the existence of 1D conducting channels in the compound [37]. However, as such a 1D conducting channel is expected along the *a* axis in $ZrTe_3$, this finding cannot explain our results. Instead, this anomalous behavior may indicate that the conventional fluctuation theory is not appropriate for our data. According to the local-pair induction scenario, the bulk SC emerges in addition to the filamentary SC. Thus, we speculate that such this mixing of two kinds of SC, that is, the unconventional mechanism of the bulk SC increases the complexity of the fluctuation phenomena. This behavior can yeild unusual excess conductivity, corresponding to deviation from the 3D AL model.

Here, we summarize the above discussions and consider the origin of the filamentary SC. In our results, the pressure dependencies of T_c (figure 3) and H_{c2} (figure 5), as well as the magnetic field angular dependence of H_{c2} (figure 6) of the filamentary SC are similar to those of the bulk SC, indicating a connection between these types of SC. These discussions are not sufficient to conclude whether the filamentary SC can be regarded as a fluctuation in the bulk SC enhanced by low dimensionality alone or local-pair-induced SC. However, the discussion of the electronic structure based on the band structure calculation [12] and ARPES measurements [31] indicates that the Q1D+3D FSs after the CDW transition are relevant to an SC emergence that favors local-pair formation. The comparison with the SC transition in $Tl_2Mo_6Se_6$ suggests that the filamentary SC in $ZrTe_3$ can be attributed to Cooper pairs characterized by extremely short coherence lengths. Moreover, the excess conductivity observed in this study (figure 7) and the anomalous specific heat [15] suggest that bulk SC fluctuation does not agree with conventional fluctuation theory. Therefore, from a comprehensive perspective, it is reasonable to conclude that our results favor the local-pair-induced SC scenario rather than conventional SC.

The H_{c2} of the filamentary SC is worth noting as it can reflect the characteristics of the local pair-induced SC. Usually, for Josephson-coupled superconductors, the H_{c2} values at low temperatures are large. In previous studies, they exceeded H_p [38, 39] when a magnetic field was applied to the Josephson-coupled SC chains or layers, because the orbital current path was enclosed by the Josephson junctions, suppressing an increase in the kinetic energy. In contrast to the behavior reported in those studies, although the SC filaments were coupled by the Josephson effect in this study, the H_{c2} curves indicate that the orbital pair-breaking effect played a dominant role in the SC. The weakness of the filamentary SC under the influence of a magnetic field may be unique to $ZrTe_3$. As the local pairs are confined within narrow SC filaments having extremely small cross-sectional area (as a result of highly 1D electronic structure of $ZrTe_3$), a critical value for the screening current can be obtained more easily than for other high-dimensional superconductors. This may be the reason why the H_{c2} curves of the filamentary SC are dominated by the orbital pair-breaking effect.

Several theoretical models of local pair-induced SC have predicted that H_{c2} is determined by the Pauli paramagnetic effect [40] and that the H_{c2} curve has upward curvature and shows no saturation behavior at low temperatures [41]. However, our results show that the H_{c2} curves are in good agreement with those expected based on consideration of the orbital effect. This discrepancy may be due to the difference in dimensionality. In all the theoretical models, a 2D electron system is assumed. However, in $ZrTe_3$, FSs in which electrons have Q1D characteristics play a crucial role. As has been discussed above, the small critical current in the filamentary SC can make a significant contribution to the behavior of the corresponding H_{c2}.

The small critical current of the filamentary SC may have an effect on the magnetic response. Previous magnetic measurements have shown that a diamagnetic signal is not observed down to 2 K [14]. This may indicate that SC filaments are not coupled, which seems to contradict our results. In the filamentary SC, the critical value of the current can be very small, and the screening current will be small even if SC filaments are coupled. This will cause difficulty in detecting the diamagnetic response in the filamentary SC.

5. Conclusion

By measuring the resistance of $ZrTe_3$ with different I configurations under an applied pressure and magnetic fields, we showed the filamentary and bulk SC nature, which shows resistive transition along the a axis at 4 K and along the other axes at 2 K. The H_{c2} curves, H_{c2} anisotropy, and pressure evolution obtained from the measurement for $I \parallel a$ were quite similar to those for $I \parallel b$, indicating that the origin of the filamentary SC can be linked to that of the bulk SC. Moreover, the bulk SC fluctuation exhibited unusual behavior. The results suggest that the emergence of filamentary and bulk SC is a consequence of local-pair formation and local-pair induced Cooper pairs.

Acknowledgments

The authors would like to thank S Yasuzuka, K Ichimura and T Matsuura for helpful discussion.

References

[1] Wilson J A, Disalvo F J and Mahajan S 1975 *Adv. Phys.* **24** 117
[2] Monceau P, Ong N P, Portis A M, Meerschaut A and Rouxel J 1976 *Phys. Rev. Lett.* **37** 602
[3] Sambongi T, Tsutsumi K, Shiozaki Y, Yamamoto M, Yamaya K and Abe Y 1977 *Solid State Commun.* **22** 729
[4] Tsutsumi K, Takagaki T, Yamamoto M, Shiozaki Y, Ido M, Sambongi T, Yamaya K and Abe Y 1977 *Phys. Rev. Lett.* **39** 1675
[5] Wise W D, Boyer M C, Chatterjee K, Kondo T, Takeuchi T, Ikuta H, Wang Y and Hudson E W 2008 *Nat. Phys.* **4** 696
[6] Hanaguri T, Lupien C, Kohsaka Y, Lee D H, Azuma M, Takano M, Takagi H and Davis J C 2004 *Nature* **430** 1001
[7] Shen K M *et al* 2005 *Science* **307** 901
[8] Chang J *et al* 2012 *Nat. Phys.* **8** 871
[9] Berthier C, Moline P and Jerome D 1976 *Solid State Commun.* **18** 1393
[10] Kawabata K 1985 *J. Phys. Soc. Japan* **54** 762
[11] Furuseth S and Fjellvag H 1991 *Acta Chem. Scand.* **45** 694
[12] Felser C, Finckh E W, Kleinke H, Rocker F and Tremel W 1998 *J. Mater. Chem.* **8** 1787
[13] Nakajima H, Nomura K and Sambongi T 1986 *Physica* B **143B** 240
[14] Takahashi S, Sambongi T and Okada S 1983 *J. Phys. (Paris) Colloq.* **44** C3-1733
[15] Yamaya K, Takayanagi S and Tanda S 2012 *Phys. Rev.* B **85** 184513
[16] Ranninger J and Robaszkiewicz S 1985 *Physica* B **135B** 468
[17] Robaszkiewicz S, Micnas R and Ranninger J 1987 *Phys. Rev.* B **36** 180
[18] Micnas R, Ranninger J and Robaszkiewicz S 1990 *Rev. Mod. Phys.* **62** 113
[19] Eiling A and Schilling J S 1981 *J. Phys. F: Met. Phys.* **11** 623
[20] Takahashi S, Sambongi T, Brill J W and Roark W 1984 *Solid State Commun.* **49** 1031
[21] Eaglesham D J, Steeds J W and Wilson J A 1984 *J. Phys. C: Solid State Phys.* **17** L697
[22] Yomo R, Yamaya K, Abliz M, Hedo M and Uwatoko Y 2005 *Phys. Rev.* B **71** 132508
[23] Clogston A M 1962 *Phys. Rev. Lett.* **9** 266
[24] Werthamer N R, Helfand E and Hohenberg P C 1966 *Phys. Rev.* **147** 295
[25] Tinkham M 1996 *Introduction to Superconductivity* (New York: McGraw-Hill)
[26] Turkevich L A and Klemm R A 1979 *Phys. Rev.* B **19** 2520
[27] Lawrence W E and Doniach S 1971 *Proc. 12th Int. Conf. on Low Temperature Physics* ed E Kanda (Japan: Academic) p 361
[28] Tinkham M 1963 *Phys. Rev.* **129** 2413
[29] Aslamazov L G and Larkin A I 1968 *Phys. Lett.* **26A** 238
[30] Yamaya K, Yoneda M, Yasuzuka S, Okajima Y and Tanda S 2002 *J. Phys.: Condens. Matter* **14** 10767
[31] Yokoya T, Kiss T, Chainani A, Shin S and Yamaya K 2005 *Phys. Rev.* B **71** 140504(R)
[32] Labble J and Friedel J 1966 *J. Phys. (Paris)* **27** 153
[33] Labble J and Bok J 1987 *Europhys. Lett.* **3** 1225
[34] Alexandrov A S, Ranninger J and Robaszkiewicz S 1986 *Phys. Rev.* B **33** 4526
[35] Bergk B, Petrovic A P, Wang Z, Wang Y, Salloum D, Gougeon P, Potel M and Lortz R 2011 *New J. Phys.* **13** 103018
[36] Petrovic A P, Ansermet D, Chernyshov D, Hoesch M, Salloum D, Gougeon P, Potel M, Boeri L and Panagopoulos C 2016 *Nat. Commun.* **7** 12262
[37] Han S H, Axnas J, Zhao B R and Rapp O 2004 *Physica* C **408** 679
[38] Yonezawa S, Kusaba S, Maeno Y, Auban-Senzier P, Pasquier C, Bechgaard K and Jerome D 2008 *Phys. Rev. Lett.* **100** 117002
[39] Kano M, Mori H, Matsubayashi K, Itoi M, Hedo M, Murphy T P, Tozer S W, Uwatoko Y and Nakamura T 2012 *J. Phys. Soc. Japan* **81** 024716
[40] Domanski T, Maska M M and Mierzejewski M 2003 *Phys. Rev.* B **67** 134507
[41] Mierzejewski M and Maska M M 2004 *Phys. Rev.* B **69** 054502